



UNIVERSITÀ POLITECNICA DELLE MARCHE  
Repository ISTITUZIONALE

Osteogenic potential of dualblocks cultured with human periodontal ligament stem cells:in vitro and synchrotron microtomography study

This is a pre print version of the following article:

*Original*

Osteogenic potential of dualblocks cultured with human periodontal ligament stem cells:in vitro and synchrotron microtomography study / Manescu, Adrian; Giuliani, Alessandra; Mohammadi, S.; Tromba, G.; Mazzoni, Serena; Diomede, F.; Zini, N.; Piattelli, A.; Trubiani, O.. - In: JOURNAL OF PERIODONTAL RESEARCH. - ISSN 0022-3484. - STAMPA. - 51:1(2016), pp. 112-124. [10.1111/jre.12289]

*Availability:*

This version is available at: 11566/226809 since: 2022-05-23T16:39:00Z

*Publisher:*

*Published*

DOI:10.1111/jre.12289

*Terms of use:*

The terms and conditions for the reuse of this version of the manuscript are specified in the publishing policy. The use of copyrighted works requires the consent of the rights' holder (author or publisher). Works made available under a Creative Commons license or a Publisher's custom-made license can be used according to the terms and conditions contained therein. See editor's website for further information and terms and conditions.

This item was downloaded from IRIS Università Politecnica delle Marche (<https://iris.univpm.it>). When citing, please refer to the published version.

(Article begins on next page)

Journal of

**PERIODONTAL RESEARCH**

**Osteogenic potential of collagenated porcine Dual-blocks cultured with periodontal ligament stem cells: an in-vitro study validated by synchrotron radiation phase-contrast microtomography**

|                               |   |
|-------------------------------|---|
| Journal:                      | <i>Journal of Periodontal Research</i>  |
| Manuscript ID:                | Draft   |
| Manuscript Type:              | Original Article  |
| Date Submitted by the Author: | n/a   |
| Complete List of Authors:     | Manescu, Adrian; Università Politecnica delle Marche, Dip. di Scienze Cliniche Specialistiche e Odontostomatologiche<br>Giuliani, Alessandra; Università Politecnica delle Marche, Dip. di Scienze Cliniche Specialistiche e Odontostomatologiche<br>Mohammadi, Sara; Sincrotrone Trieste S.C.p.A,<br>Tromba, Giuliana; Sincrotrone Trieste S.C.p.A,<br>Mazzoni, Serena; Università Politecnica delle Marche, Dip. di Scienze Cliniche Specialistiche e Odontostomatologiche<br>Diomede, Francesca; University "G. d'Annunzio", Department of Medical, Oral and Biotechnological Sciences<br>Piattelli, Adriano; University "G. d'Annunzio", Department of Medical, Oral and Biotechnological Sciences<br>Trubiani, Oriana; University "G. d'Annunzio", Department of Medical, Oral and Biotechnological Sciences |
| Keywords:                     | Tissue Engineering, Stem Cells, Periodontal ligament, Biomaterial   |
|                               |   |

SCHOLARONE™  
Manuscripts

Osteogenic potential of collagenated porcine Dual-blocks cultured with periodontal  
ligament stem cells: an in-vitro study validated by synchrotron radiation phase-contrast  
microtomography

Osteogenic potential of hPDLSC cultured scaffolds

A. Manescu<sup>1</sup>, A. Giuliani<sup>1\*</sup>, S. Mohammadi<sup>2</sup>, G. Tromba<sup>2</sup>, S. Mazzoni<sup>1</sup>, F. Diomedea<sup>3</sup>,  
A. Piattelli<sup>3</sup>, O. Trubiani<sup>3</sup>

<sup>1</sup>Università Politecnica delle Marche, Dipartimento di Scienze Cliniche Specialistiche e  
Odontostomatologiche – Sezione di Biochimica, Biologia e Fisica, Via Brece Bianche  
1, 60131 Ancona, Italy

<sup>2</sup>Sincrotrone Trieste S.C.p.A, Strada Statale 14 - km 163.5 in AREA Science Park,  
34149 Basovizza (Trieste), Italy

<sup>3</sup> University of Chieti-Pescara, Department of Medical, Oral and Biotechnological  
Sciences, Laboratory of Stem Cells and Regenerative Medicine, Via dei Vestini 31,  
66100 Chieti, Italy

\* Corresponding author: Alessandra Giuliani, Università Politecnica delle Marche,  
Dipartimento di Scienze Cliniche Specialistiche e Odontostomatologiche – Sezione di  
Biochimica, Biologia e Fisica, Via Brece Bianche 1, 60131 Ancona, Italy, Tel. +39  
071 2204603, Fax. +39 071 2204605, Email: a.giuliani@univpm.it

## Abstract

Objective: In the present study, the early stages of *in vitro* bone formation in collagenated porcine scaffolds cultured with Periodontal Ligament Cells (hPDLSCs) were investigated. The comparison between the osteogenic potential of this structure in basal and differentiating culture media was explored to predict the mechanism of its biological behavior as graft in human defect. Results were validated by Synchrotron Radiation X-ray phase contrast micro computed tomography (SR micro-CT).

Background: The restoration of large bony maxillofacial defects represents one of the tissue engineering main challenges. It has been recently explored using cells and tissues developed *in vitro* that should ideally be immunologically, functionally, structurally and mechanically identical to the native tissue.

Method: *In vitro* cultures of human PDLSCs, easily obtained by scraping of alveolar crestal and horizontal fibers of the periodontal ligament, were seeded onto collagenated porcine blocks constituted by natural cancellous and cortical bone. 3D images were obtained by SR micro-CT and processed with the phase-retrieval algorithm based on the Transport of Intensity Equation (TIE).

Results: This work proved the *in-vitro* osteogenic potential of collagenated Dual-Blocks cultured with hPDLSCs (regardless of the culture medium) and demonstrate the capability of phase-contrast micro-CT analysis to study newly bone formation on collagenated bioscaffolds.

Conclusion: The chosen method successfully and quantitatively monitored the early stages of bone formation and the rate of the bioscaffold resorption in basal and differentiating culture media.

1  
2  
3  
4  
5  
6  
7  
8  
9  
10  
11  
12  
13  
14  
15  
16  
17  
18  
19  
20  
21  
22  
23  
24  
25  
26  
27  
28  
29  
30  
31  
32  
33  
34  
35  
36  
37  
38  
39  
40  
41  
42  
43  
44  
45  
46  
47  
48  
49  
50  
51  
52  
53  
54  
55  
56  
57  
58  
59  
60

**Keywords:** Human periodontal ligament stem cells; bone regeneration; phase contrast tomography; synchrotron radiation.

Manuscript proof

## 1. Introduction

Large bony maxillofacial defects are currently repaired by free tissue transfer with microvascular reanastomosis of vascularized flaps from distant sites including fibula, iliac crest, scapula, and radius (1, 2). These procedures have proven to be reliable and effective but require extended hospitalization and a secondary donor site where associated morbidity and complications could occur (3). Bone tissue engineering combined to gene therapy and stem cell biology is considered a promising alternative to the autologous approach. Manipulating cells, biomaterial scaffolds and cell signaling factors to regenerate large skeletal defects offers several potential benefits, including the lack of donor site, morbidity, decrease in technical sensitivity of the repair, and most importantly, the ability to closely mimic the *in vivo* microenvironment.

The restoration of damaged functions represents the main goal of contemporary medical research, using cells and tissues developed *in vitro* that should ideally be immunologically, functionally, structurally and mechanically identical to the native tissue.

However, the affirmation stating that the optimal bone construct for repair would exactly replicate the lost structure is very controversial. Indeed, if this statement is well accepted in standard tissue conditions, clinical cases presenting defects with compromised tissue beds, like in the elderly or in patients with bone reabsorption caused by disease, suggest innovative approaches (4).

Recent reports have shown that many adult tissues contain a population of stem cells (SCs) identified in the stromal tissue like bone marrow, spleen, and thymus. These are postnatal stem cells able to self-renew and regenerate lineages as bone, cartilage, tendon, skeleton muscle, neuron and oral tissue<sup>5</sup>.

1  
2  
3  
4 In particular, a stem cells population found in the human periodontal ligament (hPDL),  
5 expressing a variety of stemness markers as CD29, CD90, CD44, CD 73, CD105,  
6 CD166, nanog, SSEA-4, oct-4, has been described (6,7).  
7  
8

9  
10 The human Periodontal Ligament Stem Cells (hPDLSCs), easily obtainable by scraping  
11 of alveolar crestal and horizontal fibers of the periodontal ligament, are receiving  
12 extensive attention for the immense potential for tissue regeneration, since exhibit high  
13 proliferative capacity, immunomodulatory property, potential to differentiate into  
14 osteogenic, adipogenic, and chondrogenic lineages, and moreover, they possess the  
15 capacity to generate new bone following ectopic transplantation (8-10).  
16  
17

18 However, a major factor hampering such endeavors is that the environment where stem  
19 cells grow or are seeded has critical but poorly understood effects on their fate (11-16).  
20  
21 Choosing chemical composition and internal structure of a scaffold are major decisions  
22 involving a variety of parameters such as phase composition, porosity, pore size and  
23 interconnectivity. These factors affect the transportation of nutrients that enable cell  
24 growth and proliferation and make the scaffold a suitable template for tissue growth  
25 and, eventually, osteodifferentiation, bone tissue formation, and vascularization (9, 17-  
26 19).  
27  
28

29 In this context, it has to be stressed that the kinetics of early stage *in vitro* bone  
30 formation is still unclear. Routine laboratory protocols typically subject tissue-  
31 engineered specimens only to histological analysis and electron microscopy  
32 examination, to characterize their constituent elements in 2D (9, 20). 3D visualization  
33 techniques have been demonstrated to achieve a greater understanding. X-ray computed  
34 microtomography (micro-CT), one of the most common 3D imaging techniques, has  
35 been applied to the qualitative and quantitative evaluation of tissue growth under  
36  
37  
38  
39  
40  
41  
42  
43  
44  
45  
46  
47  
48  
49  
50  
51  
52  
53  
54  
55  
56  
57  
58  
59  
60

1  
2  
3  
4 different conditions, including engineered bone (4, 14, 16-19, 21) and tendon (22).  
5  
6 However, data regarding the application of X-ray-based techniques to complex  
7  
8 constructs such those referred to early stages of *in vitro* culture of collagenated scaffolds  
9  
10 cultured with stem cells are still limited. Whereas soft tissue investigation by  
11  
12 attenuation-based X-ray imaging methods without contrast agents is hampered by poor  
13  
14 contrast, phase-sensitive techniques afford enhanced contrast where absorption is  
15  
16 insufficient, for instance to detect cells, extracellular matrix (ECM) and vessel  
17  
18 structures. Phase-contrast X-ray imaging (PCI) is sensitive to light elements such as  
19  
20 hydrogen, carbon, nitrogen and oxygen, which are commonly found in soft tissue. The  
21  
22 phase contrast arises because both the amplitude and phase are modified as the X-ray  
23  
24 beam propagates through tissue. Since the probability for X-ray phase shift can be 1000  
25  
26 times greater than for X-ray attenuation in the keV energy range, PCI affords  
27  
28 visualization of soft tissues with identical or similar attenuation characteristics, which  
29  
30 would not be detected using conventional attenuation-based imaging methods.  
31  
32 Moreover, because the refractive index-based image contrast decreases less rapidly with  
33  
34 increasing X-ray energy compared with attenuation-based contrast, PCI enables  
35  
36 reduction of the delivered radiation dose (23).

37  
38 Unfortunately the simpler PCI settings do not automatically provide quantitative phase  
39  
40 data, meaning that phase-retrieval algorithms (24-26) are often required.

41  
42 In this work we showed the *in-vitro* osteogenic potential of collagenated Dual-Blocks  
43  
44 cultured with hPDLSCs, regardless of the culture medium. We also demonstrated that  
45  
46 PCI micro-CT combined with a single distance phase-retrieval algorithm is a suitable  
47  
48 method to study *in vitro* the early stages of bone formation. In this direction the present  
49  
50  
51  
52  
53  
54  
55  
56  
57  
58  
59  
60

1  
2  
3  
4 research offers a new approach with a clinical advantage in the evaluation of  
5  
6 regenerative cranio-facial surgery.  
7  
8

## 9 10 11 **2. Materials and methods**

### 12 13 **2.1. Scaffold material**

14  
15 The scaffold material is named OsteoBiol® Dual-Block (TecnoSS® Dental, Coazze  
16  
17 (TO), Italy). It is a collagenated porcine block constituted by natural cancellous and  
18  
19 cortical bone. The peculiarity is represented by the cortical bone which is naturally  
20  
21 anchored to cancellous bone in order to provide stability after grafting. This scaffold  
22  
23 guarantees, due to its rigid consistency, that the original volume of grafting site can be  
24  
25 preserved. It is indicated for horizontal crest reconstructions.  
26  
27

### 28 29 **2.2. Isolation and culture of human Periodontal Ligament Stem Cells (hPDLSCs).**

30  
31 The hPDLSCs were obtained from fragments of periodontal ligament tissue from third  
32  
33 molar teeth, scheduled to be removed for orthodontic purposes. Teeth were selected  
34  
35 from healthy patients ranging from 20 to 35 years old. Before extraction, each subject  
36  
37 underwent complete medical anamnesis for systemic and oral infections or diseases. All  
38  
39 patients provided written consent for clinical research and for the processing of personal  
40  
41 data. All teeth samples were de-identified. The periodontal ligament tissue was  
42  
43 collected after tooth extraction. Explants were obtained from alveolar crestal and  
44  
45 horizontal fibers of the periodontal ligament by scraping the roots of non-carious third  
46  
47 molar teeth with a Gracey's curette (27).  
48  
49

50  
51 The hPDLSCs were cultured in MSCM medium (Lonza Verviers Company, Basel,  
52  
53 Belgium) according to *Trubiani et al* (10). Briefly, the adherent cells migrating from the  
54  
55 explants were isolated using 0.1% trypsin solution and plated in tissue culture  
56  
57  
58  
59  
60

1  
2  
3  
4 polystyrene flasks at  $1 \times 10^3$  cells/cm<sup>2</sup>. Primary cultures of PDLSCs mainly consisted of  
5  
6 colonies of bipolar fibroblastoid cells which, after subcultivation, proliferate with a  
7  
8 population-doubling time of 48 h reaching a confluent growth-arrested condition.  
9

10  
11 Confluent hPDLSCs were divided in 4 different type of cultures: hPDLSCs cultured  
12  
13 without Dual-Block in MSCM medium (ctrl@group); hPDLSCs cultured without Dual-  
14  
15 Block in MSCM medium supplemented with hMSC Osteogenic single quotes (Lonza)  
16  
17 (Diff@group); hPDLSCs cultured with Dual-Block in MSCM medium (DB-  
18  
19 ctrl@group); hPDLSCs cultured with Dual-Block in MSCM medium supplemented  
20  
21 with hMSC Osteogenic single quotes (DB-Diff@group).  
22

23  
24 The cells were seeded at  $3 \times 10^3$  cells/cm<sup>2</sup>, the medium was changed every 3 days and at  
25  
26 each medium change the culture was examined to be sure that the monolayer was intact.  
27

28  
29 After 3 weeks of incubation the progressive mineralization was evaluated.

30  
31 All experiments were carried out using cells at the 2<sup>nd</sup> passage and repeated with 3  
32  
33 different cell samples from 3 different patients.  
34

### 35 **2.3. Cytofluorimetric assay**

36  
37 Antibodies. Fluorescein isothiocyanate-conjugated anti-CD13 (CD13 FITC),  
38  
39 phycoerythrin-conjugated anti-CD29 (CD29 PE), FITC-conjugated: anti-CD44 (CD44  
40  
41 FITC), anti-CD45 (CD45 FITC), anti-CD105 (CD105 FITC) and anti-CD166 (CD166  
42  
43 FITC) were obtained from Ancell (MN, USA); FITC-conjugated anti-CD14 (CD14  
44  
45 FITC) and PE-conjugated anti-CD133 (CD133 PE) were purchased from Milteny  
46  
47 Biotec (Bergisch Gladbach, Germany); PE-conjugated anti-CD73 (CD73 PE), FITC-  
48  
49 conjugated anti-CD90 (CD90 FITC), allophycocyanin-conjugated anti-CD117 (CD117-  
50  
51 APC), PE-conjugated anti-CD146 (CD146 PE), PE-conjugated anti-CD271 (CD271-  
52  
53 PE), Alexa488-conjugated anti-Sox2 (Sox2 Alexa488), FITC-conjugated anti-SSEA4  
54  
55  
56  
57  
58  
59  
60

1  
2  
3  
4 (SSEA4 FITC), Alexa488-conjugated anti-HLA ABC (HLA-ABC Alexa488), PE-  
5 conjugated anti-HLA-DR (HLA-DR PE) and PE-conjugated anti-OCT3/4 (OCT3/4 PE)  
6  
7  
8 obtained from Becton Dickinson (BD, San Jose, CA); FITC-conjugated anti-CD144  
9  
10 (CD144-FITC) was obtained from Acris Antibodies (Herford, Germany); PE-  
11  
12 conjugated anti-CD34 (CD34-PE) was purchased from Beckman Coulter (Fullerton,  
13  
14 CA, USA); appropriate secondary FITC-conjugated antibody was obtained from  
15  
16 Jackson Immunoresearch Laboratories (West Grove, PA, USA).  
17  
18  
19

#### 20 21 22 **2.4. Cell Staining for Flow Cytometry**

23  
24 Washing buffer (phosphate buffered saline, PBS, 0.1 % sodium azide and 0.5 % bovine  
25  
26 serum albumine, BSA) was used for all washing steps (3 ml of washing buffer and  
27  
28 centrifugation, 400 xg 8 min at 4°C). Briefly, 5 x 10<sup>5</sup> cells/sample were incubated with  
29  
30 100 µl of 20 mM ethylenediaminetetraacetic acid (EDTA) at 37°C for 10 min and  
31  
32 washed.  
33

34  
35 Staining of surface antigens and intracellular antigens was carried out according to  
36  
37 *Eleuterio et al.*(6)  
38

#### 39 40 **2.5. Flow Cytometry Measurement**

41  
42 Quality control included regular check-up with Rainbow Calibration Particles (BD  
43  
44 Biosciences). Debris was excluded from the analysis by gating on morphological  
45  
46 parameters; 20,000 non-debris events in the morphological gate were recorded for each  
47  
48 sample. To assess non-specific fluorescence we used specific irrelevant controls. All  
49  
50 antibodies were titrated under assay conditions and optimal photomultiplier (PMT)  
51  
52 gains were established for each channel. Data were analysed using FlowJo™ software  
53  
54  
55  
56  
57  
58  
59  
60

(TreeStar, Ashland, OR). Mean Fluorescence Intensity Ratio (MFI Ratio) was calculated dividing the MFI of positive events by the MFI of negative events.

## 2.6. MTT assay and Trypan blue exclusion test

The viability of hPDLSCs, in control cultures (ctrl) and seeded onto Dual-Block scaffolds (DB-ctrl), was measured by the quantitative colorimetric MTT (3-[4,5-dimethyl-2-thiazolyl]-2,5-diphenyl-2Htetrazoliumbromide test) (CellTiter 96<sup>®</sup>, Promega, Milan, Italy).  $2 \times 10^2$  cells/well were seeded into a 96-well culture plate with MSCM medium. After 24 h of incubation at 37°C, 15  $\mu$ l/well of MTT was added to culture medium, and cells were incubated for 3 hrs at 37°C. The supernatants were read at 650 nm wavelength using a microplate reader (Sinergy HT, Biotek Instruments, Winooski, VT, USA). The MTT assay was performed in three independent experiments, six replicate wells for 24, 48, 72h and 1 week. Additionally, cell viability and proliferation were evaluated at 24, 48, 72 h and 1 week by trypan blue staining. Cells were analysed by an inverted light microscope (Leica DMIL; Leica Microsystems S.p.A., Milan, Italy). Dead cells would take up dyes and were stained blue, and surviving cells would be refractive without taking up dyes.

## 2.7. Preparation for scanning electron microscopy

The samples were fixed for 1 h at 4 °C in 2.5 % glutaraldehyde in 0.1M cacodylate buffer (pH 7.4), dehydrated in increasing ethanol concentrations and then critical point-dried. They were then mounted on aluminium stubs and gold-coated in an Emitech K550 (Emitech Ltd., Ashford, UK) sputter-coater before imaging by means of a scanning electron microscopy (EVO 50; ZEISS, Germany).

## 2.8. Immunofluorescence staining and confocal laser scanning microscope analysis

1  
2  
3  
4 Cells grown on glass coverslips were fixed for 10 min at room temperature (RT) with  
5  
6 4% paraformaldehyde in 0.1M sodium phosphate buffer (PBS), pH 7.4. Briefly,  
7  
8 hPDLSCs grown on Dual-Block sections were permeabilized with 0.5% Triton X-100  
9  
10 in PBS for 10 min, followed by blocking with 5% skimmed milk in PBS for 30 min.  
11  
12 Primary monoclonal antibodies to anti-human vinculin (Santa Cruz Biotechnology,  
13  
14 Santa Cruz, CA; USA) was used, followed by Alexa Fluor 488 green fluorescence  
15  
16 conjugated goat anti-mouse as secondary antibodies (Molecular Probes, Invitrogen,  
17  
18 Eugene, OR, USA). Subsequently, the sample was incubated with Alexa Fluor 594  
19  
20 phalloidin red fluorescence conjugate (1:500, Molecular Probes), as a marker of the  
21  
22 actin cytoskeleton, and TOPRO for nuclei staining (1:100, Molecular Probes). Samples  
23  
24 were visualized using a Zeiss (Jena, Germany) LSM510 META confocal system,  
25  
26 connected to an inverted Zeiss Axiovert 200 microscope equipped with a Plan Neofluar  
27  
28 oil-immersion objective (40×/1.3 NA). Images were collected using an argon laser beam  
29  
30 with excitation lines at 488 nm and a helium-neon source (543 nm and 665 nm).  
31  
32  
33

### 34 35 **2.9. Mineralization assay**

36  
37 Mineralization in hPDLSC-cultures was determined by Alizarin Red S staining. The  
38  
39 experiments were carried out in quadruplicate into a 6-well culture plate. Briefly cells  
40  
41 from each patient were allowed to grow in basal (MSCM) or differentiation osteogenic  
42  
43 (MSCM supplemented with hMSC Osteogenic single quotes) medium for 21 days with  
44  
45 and without the collagenated Dual-Block biomaterial. Samples were fixed for 1h in 4%  
46  
47 paraformaldehyde in 0.1M PBS, pH 7.4, washed three times with PBS (pH 7.4), then  
48  
49 stained with 0.5% Alizarin Red S in H<sub>2</sub>O, pH 4.0, for 20 min at room temperature.  
50  
51

52  
53 After staining, the cultures were washed three times with H<sub>2</sub>O followed by 70% ethanol.  
54  
55  
56  
57  
58  
59  
60

1  
2  
3  
4 For staining quantification of the mineralization process, samples were treated as  
5  
6 previously described<sup>28</sup>. Briefly, 800µl 10 % (v/v) acetic acid were added to each well;  
7  
8 cells were incubated for 30 min with shaking, then removed by scraping, transferred  
9  
10 into a 1.5-mL vial and vortexed for 30 s. The obtained suspension was coated with 500  
11  
12 µl mineral oil (Sigma–Aldrich, St. Louis, MO, USA), heated to 85 °C for 10 min, then  
13  
14 transferred to ice for 5 min, carefully avoiding the opening of the tubes until fully  
15  
16 cooled, and centrifuged at 20,000 × g for 15 min. The samples were acidified (pH  
17  
18 between 4.1 and 4.5) with 200 µl of 10 % (v/v) ammonium hydroxide. Aliquots (150 µl)  
19  
20 were read in triplicate at 405 nm by a spectrophotometer ND-1000 NanoDrop  
21  
22 Spectrophotometer (NanoDrop Technologies, Rockland, DE, USA).  
23  
24  
25

#### 26 **2.10. Western Blot analysis**

27  
28 After three weeks of culture cells were lysated in RIPA buffer (1x PBS, 1% Igepal, 0.5%  
29  
30 sodium deoxycholate, 0.1% sodium dodecyl sulphate (SDS) and 10µg/ml  
31  
32 phenylmethylsulfonyl fluoride (PMSF), 10 µg/ml leupeptin and 10 µg /ml soybean  
33  
34 trypsin inhibitor as inhibitors). The level of recovered protein was measured  
35  
36 spectrometrically according to the instructions of the manufacturer using the Bio-Rad  
37  
38 Protein Assay (detergent compatible) (Hercules, CA, USA).  
39  
40

41  
42 Subsequently, 30µg of protein separated on SDS-PAGE, was transferred to  
43  
44 nitrocellulose sheets using a semidry blotting apparatus. Sheets were saturated for 60  
45  
46 min at 37°C in blocking buffer (PBS supplemented with 5% skimmed milk), then  
47  
48 incubated overnight at 4°C in blocking buffer containing primary antibodies such as:  
49  
50 collagen type I, and β-actin type I (Santa Cruz Biotechnology, Santa Cruz, CA, USA).  
51  
52

53 They were incubated for 30 min at room temperature with HPR conjugated secondary  
54  
55  
56  
57  
58  
59  
60

1  
2  
3  
4 antibody diluted 1:5.000. Bands were visualized by the ECL method; using Alliance 2.7  
5  
6 (UVItec Limited, Cambridge, UK).  
7

### 8 9 **2.11. SR X-ray phase contrast micro-CT**

10 The X-ray tomographic experiments were performed at the SYRMEP beamline  
11 (ELETTRA synchrotron light source, Trieste, Italy). The samples were investigated  
12 using isometric voxel with edge size of 9  $\mu\text{m}$ ; exposure time of 900 ms/projection; and  
13 X-ray beam energy of 16 keV, which was preliminarily found to provide acceptable  
14 imaging of both collagenated scaffold and cells while at the same time minimizing the  
15 thermal effect (reducing the absorption signal with energy increase). The sample-  
16 detector distance of 150 mm enabled to work in phase contrast mode with the typical  
17 edge enhancement feature.  
18  
19  
20  
21  
22  
23  
24  
25  
26  
27

28 The approach used in this work, i.e. phase-contrast in the edge enhancement regime,  
29 differs from conventional X-ray imaging because the resulting images are not based  
30 solely on attenuation contrast. The effect of an X-ray beam going through the sample is  
31 described by the refractive index,  $n(r) = 1 - \delta(r) + i\beta(r)$ , where  $\delta$  is the refractive index  
32 decrement and  $\beta$  is the attenuation index. As  $\delta$  is much larger than the imaginary part  $\beta$ ,  
33 the phase approach provides greater sensitivity than the absorption approach.  $\delta$  is  
34 actually proportional to the mean electron density, which in turn is nearly proportional  
35 to the mass density.  
36  
37  
38  
39  
40  
41  
42  
43  
44  
45

46 The method used for quantitative volumetric reconstructions of the refractive index is  
47 based on a two-step approach: first, the phase projections are determined in the form of  
48 Radon projections (phase retrieval) and then the object function, i.e. the refractive index  
49 decrement  $\delta$ , is reconstructed by applying a conventional filtered back projection (FBP)  
50 algorithm.  
51  
52  
53  
54  
55  
56  
57  
58  
59  
60

1  
2  
3  
4 Typically the phase retrieval implies the reconstruction of two different real-valued 3D  
5  
6 distributions,  $\delta(r)$  and  $\beta(r)$ ; such reconstruction generally requires acquisition of at least  
7  
8 two different 2D projections at each view angle. However, in some cases, it can be  
9  
10 shown *a priori* that the distributions of the real and imaginary parts of the refractive  
11  
12 index are proportional to each other, i.e.,  $\beta(r) = \varepsilon \delta(r)$ , where the proportionality  
13  
14 constant  $\varepsilon$  does not depend on the spatial coordinates. This assumption is possible only  
15  
16 for special classes of objects, such as *pure-phase* (i.e. very weakly absorbing) objects,  
17  
18 or *homogeneous* objects, such as objects consisting predominantly of a single material  
19  
20 (possibly, with a spatially varying density) (29). This last case is represented by our  
21  
22 samples where, at the early stages of bone formation in the different culture medias,  
23  
24 there is a slow variation of the complex amplitude (“monomorphous” specimen). In this  
25  
26 situation, a single projection per each view angle is sufficient for reconstruction of the  
27  
28 3D distribution of the complex refractive index (30).  
29  
30  
31  
32

33 In this study, a phase-retrieval algorithm based on the Transport of Intensity equation  
34  
35 (TIE) (29, 31) was applied to the acquired datasets with parameters tuned to edge  
36  
37 enhancement reduction and balance noise minimization. Then the common filtered  
38  
39 back-projection algorithm was used to reconstruct the slices. The X-TRACT software  
40  
41 (CSIRO Mathematical and Information Sciences, Canberra, Australia) was applied for  
42  
43 both the TIE-based phase retrieval and the reconstruction of X-ray phase-contrast slices.  
44  
45 The different phases shown in the histogram, where the different grey values  
46  
47 (proportional to  $\delta$ ) are reconstructed, were colored using a 3D display software to make  
48  
49 them easier to distinguish. Volume rendering is a 3D visualization method by which  
50  
51 data volumes are rendered directly, without the need for decomposition into geometric  
52  
53 primitives. The commercial software VG Studio MAX 1.2 (Volume Graphics,  
54  
55  
56  
57  
58  
59  
60

1  
2  
3  
4 Heidelberg, Germany) was used to generate 3D images and visualize the phase  
5  
6 distribution in 3D. Optimal image quality settings were obtained using the Scatter HQ  
7  
8 algorithm with an oversampling factor of 5.0 and activated color rendering. X-ray  
9  
10 contrast differences within samples translate into different peaks in the grey level scale,  
11  
12 corresponding to the different phases. The volume of each phase is obtained by  
13  
14 multiplying the volume of a voxel ( $\sim 730 \mu\text{m}^3$ ) by the number of voxels underlying the  
15  
16 peak associated with the relevant phase. The Mixture Modeling algorithm (NIH ImageJ  
17  
18 Plugin) was implemented to threshold the histograms. Thresholded slices were used to  
19  
20 automatically separate the new cell-derived phase from the scaffold phase. The  
21  
22 threshold of the newly formed phase (mineralized bone) was  $\sim 115$ .  
23  
24

25  
26 A structural analysis of the trabecular structure (including scaffold and newly formed  
27  
28 bone phases) was performed in order to verify if hPDLSC-culture in the two medias  
29  
30 induced morphometric modification of the templates. The following morphometric  
31  
32 parameters were evaluated: Anisotropy Degree (DA); Connectivity Density, i.e. number  
33  
34 of trabeculae per unit volume (Conn.D. – expressed in  $\text{pixel}^{-3}$ ); Mean Trabecular  
35  
36 Thickness (TbTh - expressed in micrometers); Mean Trabecular Separation (TbSp -  
37  
38 expressed in micrometers); Mean Trabecular Number (TbNr – per millimeter); Sample  
39  
40 Volume (SV) to Total Volume (TV) ratio (SV/TV – expressed as a percentage).  
41  
42

43  
44 The Degree of Anisotropy (DA) is a measure of how highly oriented the substructures  
45  
46 are within a certain volume. Trabecular structure could vary its orientation depending  
47  
48 on hPDLSC-culture and can become anisotropic. We used the mean intercept length  
49  
50 (MIL) method for determining anisotropy (32, 33). DA is calculated as  $1 - \text{length of the}$   
51  
52  $\text{shortest axis} / \text{length of the longest axis}$ , resulting in  $0 = \text{fully isotropic structure}$ ;  $1 =$   
53  
54  $\text{fully anisotropic structure}$ .  
55  
56  
57  
58  
59  
60

## 2.12. Data and statistical analysis

Statistical analysis was performed using Graph Pad Prism 4 (Graph Pad Software Inc., San Diego, CA, USA). The results were presented as means  $\pm$  standard errors of the mean (SEM). Groups of data were compared with analysis of variance (two-way ANOVA) followed by Tukey's multiple comparison tests. P values  $\leq$  0.05 were considered statistically significant.

## 3. Results

### 3.1. Cells culture

*In vitro* cell cultures are an ideal tool to investigate and compare different biomaterial scaffolds; in this context the current study assessed the cellular response to 3-D Dual-Block biomaterial.

Human PDLSCs used in this experimental protocol exhibited a cell-surface stem cell antigen phenotype positive for CD29, CD90, CD44, CD73, CD105, CD146, CD166, Oct 3/4, HLA-ABC, Sox-2 and SSEA-4 (Figure 1, section A). The proliferation rate and viability of the hPDLSCs was investigated performing an MTT and Trypan Blue exclusion test at 24, 48, 72h and 1 week of culture. Both analyses showed that the cells seeded on the dual-block showed a slightly lower growth at all examined time-points (Figure 1, section B and C).

### 3.2. Morphological analysis

SEM observations facilitated to clarify the performance of the cells/ biomaterial construct. Scanning electron microscopy (SEM) morphological analysis of Dual Block was carried out before hPDLSCs seeding. The biomaterial exhibited the characteristic

1  
2  
3  
4 aspect represented by cortical bone anchored to cancellous bone (Figure 2, section A).

5  
6 The commercially biomaterial block is shown in the inset of the Figure 2 (section A1).

7  
8 Primary hPDLSCs cells, exhibiting long processes and fibroblast-like morphology, were  
9  
10 evident at ultrastructural level (Figure 2, section B). After 24 h of incubation in presence  
11  
12 of the biomaterial no significant difficulty in the adhesiveness process was evident, in  
13  
14 fact a confluent cellular multilayer adhering directly on the cortical and cancellous  
15  
16 biomaterial confirmed the high biocompatibility of the analyzed scaffold (Figure 2,  
17  
18 section C).

19  
20  
21 At higher magnification, contact zone established through extending cytoplasmic  
22  
23 processes and filopodia, which enabled the anchorage of the cells, was shown; the distal  
24  
25 end of the filopodia and cytoplasmic processes were directly associated with the  
26  
27 constituent part of the biomaterial (Figure 2, section D). The immunohistochemistry  
28  
29 results showed that a specific positivity to vinculin was present on 3D scaffold  
30  
31 indicating an intimate contact between cells and biomaterial (Figure 2, section E, F, G  
32  
33 and H).

### 37 38 **3.3. Osteogenic Differentiation**

39  
40 At 21 days of culture the observation of cells stained with Alizarin Red S, revealed  
41  
42 newly deposited bone in Diff@group (Figure 3, section A2). In presence of biomaterial  
43  
44 a strong osteogenic induction was present in both DB-ctrl@group ad DB-Diff@group  
45  
46 (Figure 3, section B1 and 2). The sensitivity of the colorimetric method obtained by the  
47  
48 extraction of the calcified mineral at low pH, permitted to evidence an intense staining  
49  
50 peak in both undifferentiated and differentiated cells seeded on 3D biomaterial (Figure  
51  
52 3, section C).

1  
2  
3  
4 Western blot analysis showed in cells induced to osteogenic differentiation and  
5 hPDLSCs seeded on biomaterial an up-regulation of collagen type I, a bone tissue-  
6 specific protein, demonstrating an evident maturation of bone cells (Figure 3, section  
7 D). Densitometric analysis confirmed the results obtained by western blot investigation  
8 (Figure 3, section E).  
9

### 10 11 12 13 14 15 **3.4. Micro-CT**

16  
17 The osteogenic potential of collagenated porcine dual-blocks cultured with hPDLSCs,  
18 statistically demonstrated by Alizarin Red S, Western blot and densitometric analysis,  
19 was validated by the quantitative data extracted by the 3D micro-CT analysis. Micro-CT  
20 was able to easily distinguish in 3D the newly formed bone phase from the collagenated  
21 porcine scaffold. Cell-medium-scaffold interactions modified the scaffold structure,  
22 thus producing images in which two different phases with different refractive index  
23 were evident. Results are given for both basal (DB-ctrl; figure 4) and differentiating  
24 (DB-Diff; figure 5) media. The scaffold and the newly formed bone were colored using  
25 3D display software to make them more easily recognizable. The scaffold structure was  
26 shown in white (figure 4-5, panels A and D), while the newly formed bone (produced  
27 by the cells grown on the bioscaffold) was depicted in magenta (figure 4-5, panels B  
28 and E).  
29  
30  
31  
32  
33  
34  
35  
36  
37  
38  
39  
40  
41  
42  
43

44 While micro-CT revealed that no significant (detectable) bone regeneration was present  
45 after the first week in both basal and differentiating media (data not shown), starting  
46 from the second week of culture the magenta phase is easily recognizable in all the  
47 scaffolds, both in basal (figure 4, panels B and E) and differentiating (figure 5, panels B  
48 and E) media. This phase seems to occur preferentially in the trabecular portion, being  
49  
50  
51  
52  
53  
54  
55  
56  
57  
58  
59  
60

1  
2  
3  
4 probably due to the higher porosity of the scaffold in this site with respect to the  
5  
6 compact areas.  
7

8  
9 A relevant quantitative result is the decrease of the cultured scaffolds mass density ( $\rho$ ,  
10 expressed in  $\text{mg}/\text{cm}^3$ ) from the first to the second week of culture, while a slight  
11 increase was observed from the second to the third week. Such evidence is observed  
12 independently if the culture is in basal (DB-ctrl) or in differentiating (DB-Diff) medium  
13 and it is confirmed by the profile of the “Intensity Counts vs. Grey Level” for the DB-  
14 ctrl (figure 6a) and the DB-diff (figure 6b) cultures. Indeed, due to the experimental  
15 phase-contrast set-up and the TIE algorithm implemented for the data analysis, the grey  
16 levels - here referred to an unsigned 8-bit scale - are proportional to the refractive index  
17 decrement  $\delta$ , that in turn is nearly proportional to the mass density  $\rho$  of the collagenated  
18 porcine scaffold.  
19  
20

21  
22 The amount of the newly formed bone (magenta phase in figure 4, panels B and E and  
23 figure 5, panels B and E) was calculated by counting the corresponding voxels  
24 underlying the peak associated with the relevant phase. The Mixture Modeling  
25 algorithm (NIH ImageJ Plugin) was implemented to threshold the histograms and to  
26 automatically separate the new bone from the scaffold phase. The obtained data were  
27 expressed as BV/TV (%), i.e. the volume ratio of the newly-formed bone structure (BV)  
28 to the total construct volume (TV). The BV/TV ratio is reported in the top-right insert of  
29 the figure 6C as a function of time from PDLSCs seeding onto the scaffold.  
30  
31 Interestingly, a comparison between the culture in basal medium (DB-ctrl) and in  
32 differentiating medium (DB-diff) showed, within the limits of the sample size, that the  
33 BV/TV ratio in differentiating medium is almost 7-fold greater than in basal medium  
34 after 2 weeks of culture and more than 10-fold greater after 3 weeks of culture.  
35  
36  
37  
38  
39  
40  
41  
42  
43  
44  
45  
46  
47  
48  
49  
50  
51  
52  
53  
54  
55  
56  
57  
58  
59  
60

1  
2  
3  
4 The color map of the newly-formed bone thickness distribution confirmed significantly  
5 lower BV/TV percentages in cultures in basal medium (Figure 4, panels C and F) with  
6 respect to those in differentiating medium (Figure 5, panels C and F). It also showed  
7 that the compact region of the scaffolds is partially mineralized only in differentiating  
8 medium, further demonstrating the differentiating process acceleration of the hPDLSCs  
9 in the DB-diff@group, with respect to the DB-ctrl@group.  
10

11  
12 To investigate more deeply the newly formed bone changes in time, the bone thickness  
13 distribution vs. the bone volume normalized to the total sample volume was also  
14 assessed. Histograms of the distribution of the bone thickness in all the investigated  
15 samples are reported in Figure 6, panel C. It is shown here that while the average bone  
16 thickness was  $\sim 130 \mu\text{m}$  in cultures made in differentiating medium, none bone  
17 formation reached this thickness in basal medium, even after three weeks of culture.  
18  
19

20  
21 A structural analysis was also performed on the spongy portion of the samples in order  
22 to verify if hPDLSC-culture in the two media induced morphometric modification of  
23 the scaffold templates. The results are reported in Figure 7. The kinetics curve presents  
24 a comparable behavior in basal and differentiating media for all the morphometric  
25 parameters considered. Furthermore, with the exclusion of the DA parameter that seems  
26 not varying significantly ( $p > 0.05$ ) in time (presenting values between 0.6 and 0.8),  
27 significant differences ( $p < 0.05$ ) were observed between the first and the second week  
28 of culture in terms of Conn.D., TbTh and SV/TV parameters, that significantly  
29 increased, and for the TbSp parameter, that consistently decreased. This evidence  
30 further demonstrates that a significant mineralization appears starting from the 2<sup>nd</sup> week  
31 of culture, as previously stated by cell staining with Alizarin red S (Figure 3C) and  
32 validated by micro-CT (Figure 4 and Figure 5).  
33  
34  
35  
36  
37  
38  
39  
40  
41  
42  
43  
44  
45  
46  
47  
48  
49  
50  
51  
52  
53  
54  
55  
56  
57  
58  
59  
60

#### 4. Discussion

A critical goal in tissue engineering is to obtain scaffolds with tailored physical, mechanical and biological properties to act as template for stem cell growth, proliferation and differentiation in newly formed bone (34). The choice of the best scaffold-culture medium matching is a major issue in order to mimic ECM architecture and biological functions. In fact scaffolds are not only required to provide mechanical support, but they are asked to carry inductive molecules, cells and supply signals to control the structure and the function of the newly formed bone. Cell adhesion to the substrate is necessary for good scaffold-cell interactions and must occur before cell spreading, division and differentiation (11, 35).

This paper presents the characterization of early-stage *in vitro* bone formation on collagenated porcine Dual-block scaffolds seeded with PDL stem cells and cultured in basal or differentiating media. Morphological analyses by light and scanning electron microscopy explained the performance of cells in contact with the collagenated Dual Block biomaterial. The analysis showed cellular proliferation of the hPDLSCs seeded on scaffold and subsequent colonization of the biomaterial. We got evidence that cells adhered to the uppermost surface of the scaffold, also establishing cellular bridges and organizing a network between the cancellous spaces. To validate the performance of the biomaterial we have explored the focal adhesion area evaluating the vinculin expression through confocal laser scanning microscopy. Previously fluorescently-tagged vinculin has been used to demonstrate that the surface features of biomaterials made of either titanium or stainless steel are critical for number, size and dynamics of focal adhesions (36) and that the focal adhesion area increases in osteogenic cells (37). In PDLSCs

1  
2  
3  
4 several anchoring junctions bind cells to the substrate, indicating the performance of  
5  
6 above-mentioned biomaterials.  
7

8 Alizarin Red S showed a mineralized extracellular matrix in presence of the scaffold  
9  
10 both in control (DB-ctrl) and, in particular in differentiating (DB-diff) cultures,  
11  
12 indicating that the collagenated Dual- Block offers an adequate support for tissue  
13  
14 reconstruction due to its biological characteristics and ability to support cell growth and  
15  
16 differentiation. The progression of osteogenic differentiation is indicated by bone-  
17  
18 related proteins, in particular collagen type 1; the upregulation of this protein in DB-ctrl  
19  
20 cells can give insights that the scaffold could be designed as co-protagonist of the cells  
21  
22 in differentiation process (7).  
23  
24

25  
26 The study is supported and validated by a demonstrative application of SR X-ray phase  
27  
28 contrast micro-CT. This analysis disclosed spotted bone deposits, detected from the  
29  
30 second week of culture in both media, onto the scaffold template with high resolution  
31  
32 and in 3D. BV/TV ratio in differentiating medium was found to be almost 7-fold greater  
33  
34 than in basal medium after 2 weeks of culture and more than 10-fold greater after 3  
35  
36 weeks of culture. The poor signal in the basal medium may be due to the fact that here  
37  
38 the cells take longer time to differentiate than in differentiating medium even if the  
39  
40 osteoinductive potential is preserved. This is also confirmed by the morphometric  
41  
42 analysis performed in the spongy volume of the samples.  
43  
44

45  
46 Interestingly, micro-CT studies revealed a mass density decrease of the scaffolds seeded  
47  
48 with hPDLSCs in both media from the first to the second week of culture, while a slight  
49  
50 increase was observed from the second to the third week. This seems to indicate that the  
51  
52 scaffold bioresorption is more accentuated up to the second week of culture. Anyhow  
53  
54 looking at scaffold changes over time is a still challenging subject and needs a  
55  
56  
57  
58  
59  
60

1  
2  
3  
4 statistically consistent sample and proper boundary conditions. More powerful detection  
5  
6 systems are needed to investigate larger scaffolds preserving and possibly increasing the  
7  
8 spatial resolution (11). This will provide reliable quantitative data when micro-CT  
9  
10 reconstructions of biostructures undergoing remodeling (like during cell adhesion,  
11  
12 proliferation and differentiation on a bioresorbable scaffold) require segmentation.

13  
14 Notably, absorption-based micro-CT is not recommended for analysis of the present  
15  
16 samples, due to low X-ray absorption by collagenated scaffolds (14). Our demonstrative  
17  
18 experiments were indeed conducted on single sample-detector distance, with a phase-  
19  
20 contrast set-up and subsequent application of a phase retrieval algorithm based on the  
21  
22 Transport of Intensity equation (TIE). The chosen method was proved to successfully  
23  
24 reconstruct the distribution of  $\delta$  in our samples that, at the early stages of bone  
25  
26 formation in the different culture medias, can be considered “monomorphous” (i.e.  
27  
28 collagenated) specimens.  
29  
30  
31

32  
33 In conclusion, this paper describes and demonstrates the osteogenic potential of  
34  
35 collagenated porcine dual-blocks cultured with periodontal ligament stem cells and  
36  
37 shows the feasibility of SR phase-contrast micro-CT analysis to study newly bone  
38  
39 formation on collagenated bioscaffolds. More generally, it provides clear evidence that  
40  
41 the non-invasive and quantitative micro-CT may be an important characterization tool  
42  
43 for bone engineering approaches.  
44  
45

#### 46 **Acknowledgements**

47  
48 The authors acknowledge the ELETTRA User Office for kindly providing beam-time,  
49  
50 Dr. Timur Gureyev, Senior Principal Research Scientist at CSIRO Materials Science  
51  
52 and Engineering (AUSTRALIA) for his fundamental suggestions during X-TRACT  
53  
54  
55  
56  
57  
58  
59  
60

1  
2  
3  
4 data analysis and Dr Ilaria Merciaro for experimental procedure on cell culture  
5  
6 (Department of Medical, Oral and Biothechnological Sciences, Chieti, Italy).  
7

8  
9 This work arises from a collaboration between COST NAMABIO partners (A.M., A.G.,  
10  
11 S.M., and A.P.) and was financed from the Program PRIN funds of Ministero  
12  
13 dell'Istruzione, Università e Ricerca (Prot. 20102ZLNJ5).  
14  
15  
16  
17  
18  
19  
20  
21  
22  
23  
24  
25  
26  
27  
28  
29  
30  
31  
32  
33  
34  
35  
36  
37  
38  
39  
40  
41  
42  
43  
44  
45  
46  
47  
48  
49  
50  
51  
52  
53  
54  
55  
56  
57  
58  
59  
60

Manuscript proof

**References**

- [1] Disa JJ, Cordeiro PG. Mandible reconstruction with microvascular surgery. 2000; 19(3):226-34.
- [2] Emerick KS, Teknos TN. State-of-the-art mandible reconstruction using revascularized free-tissue transfer. *Expert Rev Anticancer Ther* 2007; 7(12): 1781–1788.
- [3] Ward BB, Brown SE, Krebsbach PH. Bioengineering strategies for regeneration of craniofacial bone: a review of emerging technologies. *Oral Diseases* 2010; 16(8): 709–716.
- [4] Giuliani A, Manescu A, Langer M, et al. Three years after transplants in human mandibles, histological and in-line HT revealed that stem cells regenerated a compact rather than a spongy bone: biological and clinical implication. *Stem Cells Transl Med* 2013; 2(4): 316-324.
- [5] Huang GT, Gronthos S, Shi S. Mesenchymal stem cells derived from dental tissues vs. those from other sources: their biology and role in regenerative medicine. *J Dent Res* 2009; 88(9): 792-806.
- [6] Eleuterio E, Trubiani O, Sulpizio M, et al. Proteome of human stem cells from periodontal ligament and dental pulp. *Plos One* 2013; 8(8): e7101.
- [7] Trubiani O, Fulle S, Traini T, et al. Functional assay, expression of growth factors and proteins modulating bone-arrangement in human osteoblasts seeded on an anorganic bovine bone biomaterial. *Eur Cell Mater* 2010 Jul 21; 20:72-83.
- [8] Yang H, Gao LN, An Y, et al. Comparison of mesenchymal stem cells derived from gingival tissue and periodontal ligament in different incubation conditions. *Biomaterials* 2013; 34(29): 7033-47.

1  
2  
3  
4 [9] Trubiani O, Orsini G, Zini N, et al. Regenerative potential of human periodontal  
5 ligament derived stem cells on three-dimensional biomaterials: a morphological report.  
6 J Biomed Mater Res A. 2008; 87(4): 986-93.  
7  
8

9  
10 [10] Trubiani O, Zalzal SF, Paganelli R, et al. Expression profile of the embryonic  
11 markers nanog, OCT-4, SSEA-1, SSEA-4, and frizzled-9 receptor in human periodontal  
12 ligament mesenchymal stem cells. J Cell Physiol.2010; 225(1): 123-31.  
13  
14

15 [11] Giuliani A, Moroncini F, Mazzoni S, et al. Polyglycolic Acid-Polylactic Acid  
16 scaffold response to different progenitor cell in vitro cultures: a demonstrative and  
17 comparative X-Ray Synchrotron Radiation Phase-Contrast Microtomography study.  
18 Tissue Eng Part C Methods. 2014 Apr; 20(4):308-16.  
19  
20

21 [12] Gomes ME, Bossano CM, Johnston CM, et al. In Vitro Localization of Bone  
22 Growth Factors in Constructs of Biodegradable Scaffolds Seeded with Marrow Stromal  
23 Cells and Cultured in a Flow Perfusion Bioreactor. Tissue Eng 2006; 12(1), 177-188.  
24  
25

26 [13] Rada T, Reis RL, Gomes ME. Adipose Tissue-Derived Stem Cells and Their  
27 Application in Bone and Cartilage Tissue Engineering. Tissue Eng Part B 2009; 15(2),  
28 113-125.  
29  
30

31 [14] Giuliani A, Fiori F, Manescu A, et al. Synchrotron Radiation and Nanotechnology  
32 for Stem Cell Research. In Ali Gholamrezanezhad eds. Synchrotron Radiation and  
33 Nanotechnology for Stem Cell Research. Stem Cells in Clinic and Research. InTech  
34 2011, Rijeka, Croatia, 683-708.  
35  
36

37 [15] Moon SU, Kim J, Bokara KK, et al. Carbon nanotubes impregnated with  
38 subventricular zone neural progenitor cells promotes recovery from stroke. Int J  
39 Nanomedicine 2012; 7: 2751–2765.  
40  
41  
42  
43  
44  
45  
46  
47  
48  
49  
50  
51  
52  
53  
54  
55  
56  
57  
58  
59  
60

1  
2  
3  
4 [16] Belicchi M, Cancedda R, Cedola A, et al. Some applications of nanotechnologies  
5 in stem cells research. *Mater Sci Eng B* 2009; *Solid State Mater Adv Technol* 165(3),  
6 139-147.  
7  
8

9  
10 [17] Cancedda R, Cedola A, Giuliani A, et al. Bulk and interface investigations of  
11 scaffolds and tissue-engineered bones by X-ray microtomography and X-ray  
12 microdiffraction. *Biomaterials* 2007; 28(15): 2505-2524.  
13  
14

15 [18] Renghini C, Giuliani A, Mazzoni S, et al. Microstructural characterization and in  
16 vitro bioactivity of porous glass-ceramic scaffolds for bone regeneration by synchrotron  
17 radiation X-ray microtomography. *J Eur Ceram Soc* 2013; 33(9): 1553- 1565.  
18  
19

20 [19] Cancedda R, Dozin B, Giannoni P, Quarto R. Tissue engineering and cell therapy  
21 of cartilage and bone. *Matrix Biol* 2003; 22(1): 81-91.  
22  
23

24 [20] Ohgushi H, Tamai S, Dohi Y, et al. In vitro bone formation by rat marrow cell  
25 culture. *J. Biomed. Mater. Res.* 1996; 32(3): 333–340.  
26  
27

28 [21] Giuliani A, Manescu A, Larsson E, et al. In Vivo Regenerative Properties of  
29 Coralline-Derived (Biocoral) Scaffold Grafts in Human Maxillary Defects:  
30 Demonstrative and Comparative Study with Beta-Tricalcium Phosphate and Biphasic  
31 Calcium Phosphate by Synchrotron Radiation X-Ray Microtomography. *Clin Implant*  
32 *Dent Relat Res.* 2013. doi: 10.1111/cid.12039. [Epub ahead of print]  
33  
34  
35  
36  
37  
38  
39  
40  
41  
42

43 [22] Gigante A, Busilacchi A, Lonzi B, et al. Purified collagen I oriented membrane for  
44 tendon repair: An ex vivo morphological study. *J. Orthop. Res.* 2013; 31(5): 738–745.  
45  
46  
47

48 [23] Arfelli F, Assante M, Bonvicini V, et al. Low-dose phase contrast X-ray medical  
49 imaging. *Phys Med Biol* 1998; 43(10), 2845–2852.  
50  
51

52 [24] Wu X, Yan A. Phase retrieval from one single phase contrast x-ray image. *Opt.*  
53 *Express* 2009; 17(13), 11187.  
54  
55  
56  
57  
58  
59  
60

- 1  
2  
3  
4 [25] Hofmann R, Moosmann J, Baumbach T. Criticality in single-distance phase  
5 retrieval, *Opt. Express* 2011; 19(27), 25881–25890.  
6  
7  
8 [26] Langer M, Cloetens P, Peyrin F. Fourier-wavelet regularization of phase retrieval  
9 in x-ray in-line phase tomography, *J. Opt. Soc. Am. A* 2009; 26(8), 1876-1881.  
10  
11 [27] Carranza FA. The Tooth-Supporting Structures. In: Newmann, editor. *Clinical*  
12 *Periodontology* 1996. Philadelphia: W. B. Saunders, 31-50.  
13  
14 [28] Gregory CA, Gunn WG, Peister A, Prockop DJ. An Alizarin red-based assay of  
15 mineralization by adherent cells in culture: comparison with cetylpyridiniumchloride  
16 extraction. *Anal Biochem.* 2004; 329(1):77-84.  
17  
18 [29] Gureyev TE, Pogany A, Paganin DM, Wilkins SW. Linear algorithms for phase  
19 retrieval in the Fresnel region, *Opt Commun* 2004; 231(1-6), 53–70.  
20  
21 [30] Gureyev TE, Paganin DM, Myers GR, et al. Phase-and-amplitude computer  
22 tomography, *Appl Phys Lett* 2006; 89(3), 034102.  
23  
24 [31] Gureyev TE, Mayo SC, Myers DE, et al. Refracting Röntgen's rays: Propagation-  
25 based x-ray phase contrast for biomedical imaging. *J Appl Phys* 2009; 105(10), 102005.  
26  
27 [32] Harrigan TP, Mann RW. Characterization of microstructural anisotropy in  
28 orthotropic materials using a second rank tensor. *J Mater Sci* 1984; 19(3): 761-767.  
29  
30 [33] Odgaard A. Three-dimensional methods for quantification of cancellous bone  
31 architecture. *Bone* 1997; 20(4): 315-28.  
32  
33 [34] Causa F, Netti PA, Ambrosio LA. Multi-functional scaffold for tissue regeneration:  
34 the need to engineer a tissue analogue. *Biomaterials* 2007; 28(34): 5093-9.  
35  
36 [35] Davies JE, Causton B, Bovell Y, et al. The migration of osteoblasts over substrata  
37 of discrete surface charge. *Biomaterials* 1986; 7(3): 231-233.  
38  
39  
40  
41  
42  
43  
44  
45  
46  
47  
48  
49  
50  
51  
52  
53  
54  
55  
56  
57  
58  
59  
60

1  
2  
3  
4  
5  
6  
7  
8  
9  
10  
11  
12  
13  
14  
15  
16  
17  
18  
19  
20  
21  
22  
23  
24  
25  
26  
27  
28  
29  
30  
31  
32  
33  
34  
35  
36  
37  
38  
39  
40  
41  
42  
43  
44  
45  
46  
47  
48  
49  
50  
51  
52  
53  
54  
55  
56  
57  
58  
59  
60

[36] Diener A, Nebe B, Luthen F, et al. Control of focal adhesion dynamics by material surface characteristics. *Biomaterials* 2005; 26(4): 383-392.

[37] Born AK, Rottmar M, Lischer S, et al. Correlating cell architecture with osteogenesis: first steps towards live single cell monitoring. *Eur Cell Mater* 2009; 18: 49-62.

Manuscript proof

## Figure Captions

Figure 1. Cytofluorimetric analysis of hPDLSCs culture. The values are expressed as mean fluorescence ratio (MFI) obtained dividing the MFI of positive events by the MFI of negative events. In section A the numeric values of MFI ratio are the mean  $\pm$  standard deviation (SD) of three separate experiments using cells at 2nd passage.

MTT assay in hPDLSCs grown in vitro under undifferentiating condition, with (DB-ctrl@group) or without biomaterial (ctrl@group), over 24h, 48h, 72h, 1 week time-points. The proliferation rate was measured as the absorbance detected at 490 nm.

Trypan blue exclusion test show the proliferation rate and viability of hPDLSCs. In both tests MTT (B) and Trypan Blue (C) the cells seeded on the dual-block showed a slightly lower growth in all examined time-points. The Y-axis shows cell number, and X-axis shows culture time. Results are expressed as mean  $\pm$ SEM of three independent experiments for each patient.

Figure 2. Scanning electron microscopy of Dual Block before grafting. (A) The cortical bone is anchored to cancellous bone; the biomaterial block, as commercially provided, is showed in the inset (A1). (B) Photomicrograph of a primary culture of human Periodontal Ligament Stem Cell (hPDLSC) line expanded ex vivo; it shows a morphological homogeneous fibroblast-like appearance with a stellate shape and elongated cytoplasmic processes. (C) Living un-induced hPDLSCs (DB-ctrl@group), after 24h of culture, grown on tridimensional scaffold. High magnification revealed hPDLSCs adhesion to substrate: in fact, confluent cells were observed on the biomaterial surface. (D) Cellular margin were indiscernible for the intimate contact

1  
2  
3  
4 between neighboring cells; cellular bridge was evident in the cancellous space. (E-H)  
5  
6 Representaive image of hPDLSCs seeded on 3D-biomaterial expressing vinculin and  
7  
8 actin. Section E (green fluorescence) showed a punctate vinculin labelling in cells  
9  
10 adhering to substrate. Rhoadamine –Phalloidin staining showed the spatial cytoskeleton  
11  
12 of human periodontal ligament stem cells (red fluorescence, F). In section G it was  
13  
14 possible to observe the nuclei stained with Topro (blue fluorescence). Section H  
15  
16 indicated merged image with the triple staining of cells seeded on biomaterial. Asterisk:  
17  
18 3D-Dual Block.  
19  
20  
21  
22  
23

24 Figure 3. The osteogenic differentiation of hPDLSCs was evaluated as extracellular  
25  
26 matrix mineralization for 21 day, in basal (A1 and B1) and osteogenic medium (A2 and  
27  
28 B2), in absence (A) or presence (B) of the collagenated biomaterial. If a mineralized  
29  
30 matrix is present in osteogenic induced cells (A2) also in absence of the scaffold, an  
31  
32 evident mineralization was detected both in basal conditions (B1) and in osteogenic  
33  
34 induction (B2) when the scaffold is present.  
35  
36

37 Mineralization of hPDLSCs, grown for 1, 2 and 3 wks under osteogenic and basal  
38  
39 conditions, with or without biomaterial, was evaluated by cell staining with Alizarin red  
40  
41 S (ARS) and quantification of staining (C) via extraction with ammonium hydroxide at  
42  
43 different commitment time. The amount of released dye is measured by a microplate  
44  
45 reader at 405 nm. The values, expressed as units of optical density (O.D.), are the mean  
46  
47  $\pm$  SEM of three independent experiments, in which different cell samples were used.  
48  
49 Immunoblotting experiments and densitometric analysis of collagen type 1 showed an  
50  
51 upregulation of protein in osteogenic induced cells respect to control. In DB-ctrl@group  
52  
53 a quantity of the collagen type 1 protein similar to DB-diff@group was present  
54  
55  
56  
57  
58  
59  
60

1  
2  
3  
4 indicating the osteoinductive properties of the biomaterial. B-actin represents an  
5  
6 housekeeping protein (D and E).  
7  
8  
9

10  
11 Figure 4. Dual block and hPDLSCs in basal medium. The interaction between cells and  
12  
13 scaffold produces 3D Micro-CT images with two different phases, corresponding to  
14  
15 different  $\delta$  (refractive index decrement) values. DB scaffolds are rendered in grey  
16  
17 (panels a, b at wk2; panels d, e at wk3), whereas the contrast produced by cells - the  
18  
19 newly-formed bone - is colored in magenta (panel b at wk2; panel e at wk3). Color map  
20  
21 of bone thickness distribution at wk2 and wk3 are given in panel c and panel f,  
22  
23 respectively. Thickness scale on the left. Bar: 500  $\mu\text{m}$ .  
24  
25  
26  
27

28  
29 Figure 5. Dual block and hPDLSCs in osteogenic medium. The interaction between  
30  
31 cells and scaffold produces 3D Micro-CT images with two different phases,  
32  
33 corresponding to different  $\delta$  (refractive index decrement) values. DB scaffolds are  
34  
35 rendered in grey (panels a, b at wk2; panels d, e at wk3), whereas the contrast produced  
36  
37 by cells - the newly-formed bone - is colored in magenta (panel b at wk2; panel e at  
38  
39 wk3). Color map of bone thickness distribution at wk2 and wk3 are given in panel c and  
40  
41 panel f, respectively. Thickness scale on the left. Bar: 500  $\mu\text{m}$ .  
42  
43  
44  
45

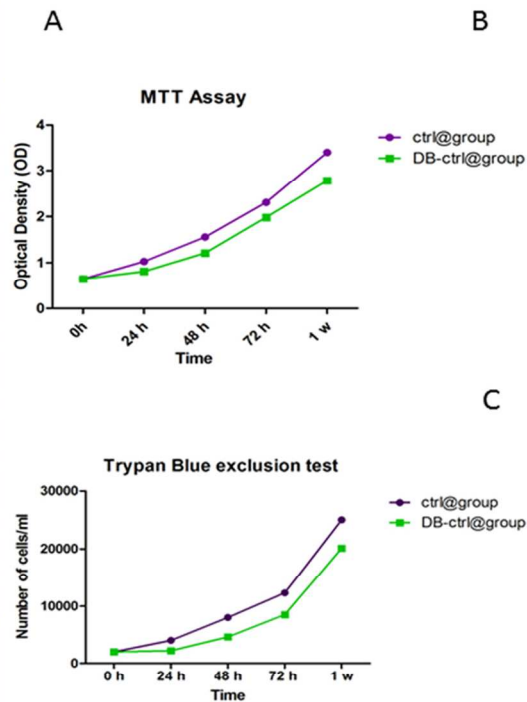
46  
47 Figure 6. (a-b) Portion of the profile of the Intensity Counts vs. Grey Levels  
48  
49 (proportional to the refractive index decrement  $\delta$ ). The integrated areas of the  
50  
51 represented peaks correspond to the collagenated porcine Dual-block volume in  
52  
53 scaffolds cultured in basal medium (panel a) and differentiating medium (panel b). In  
54  
55 both media the contrast produced at wk2 of culture is lower than for wk1, but increases  
56  
57  
58  
59  
60

1  
2  
3  
4 from wk2 to wk3. (c) Histograms of the distribution of the bone thickness in all the  
5 investigated samples at wk2 and wk3 of culture. The volume ratio (= BV/TV) of the  
6 newly-formed bone structure (BV) to the total construct volume (TV) is reported in the  
7 top-right insert.  
8  
9  
10  
11  
12  
13  
14

15 Figure 7. Morphometric parameters investigated in scaffolds cultured with hPDLSCs,  
16 both in basal and differentiating media, after 1, 2 and 3 wks of culture: Anisotropy  
17 Degree (DA); Connectivity Density (Conn.D. – expressed in  $\text{pixel}^{-3}$ ); Mean Trabecular  
18 Thickness (TbTh - expressed in micrometers); Mean Trabecular Separation (TbSp -  
19 expressed in micrometers); Mean Trabecular Number (TbNr – per millimeter); Sample  
20 Volume (SV) to Total Volume (TV) ratio (SV/TV – expressed as a percentage).  
21  
22  
23  
24  
25  
26  
27  
28  
29  
30  
31  
32  
33  
34  
35  
36  
37  
38  
39  
40  
41  
42  
43  
44  
45  
46  
47  
48  
49  
50  
51  
52  
53  
54  
55  
56  
57  
58  
59  
60

| Flow cytometry hPDLSCs |     |                    |
|------------------------|-----|--------------------|
| Antigens               |     | MFI Ratio $\pm$ SD |
| CD13                   | +   | 8,3 $\pm$ 3,5      |
| CD14                   | -   | 1,4 $\pm$ 0,2      |
| CD29                   | ++  | 62,9 $\pm$ 3,2     |
| CD34                   | -   | 1,4 $\pm$ 0,2      |
| CD44                   | ++  | 24,5 $\pm$ 2,3     |
| CD45                   | -   | 1,4 $\pm$ 0,3      |
| CD73                   | ++  | 41,7 $\pm$ 3,4     |
| CD90                   | +++ | 160,1 $\pm$ 15,6   |
| CD105                  | +   | 25,5 $\pm$ 2,3     |
| CD117                  | +/- | 4,2 $\pm$ 0,8      |
| CD133                  | -   | 2,1 $\pm$ 0,4      |
| CD144                  | -   | 1,2 $\pm$ 0,1      |
| CD146                  | +   | 11,5 $\pm$ 1,3     |
| CD166                  | +   | 8,4 $\pm$ 0,6      |
| CD271                  | -   | 1,3 $\pm$ 0,3      |
| HLA-ABC                | +++ | 121,3 $\pm$ 18,2   |
| HLA-DR                 | -   | 1,1 $\pm$ 0,1      |
| OCT3/4                 | +   | 37,6 $\pm$ 0,4     |
| Sox-2                  | +++ | 103,2 $\pm$ 7,9    |
| SSEA-4                 | ++  | 33,6 $\pm$ 2,7     |

- negative expression; +/- low expression; + moderate expression; ++ positive; +++ high expression; MFI Ratio is the average of five different biological samples  $\pm$  standard deviation; Cutoff Ratio positivity >2.0.

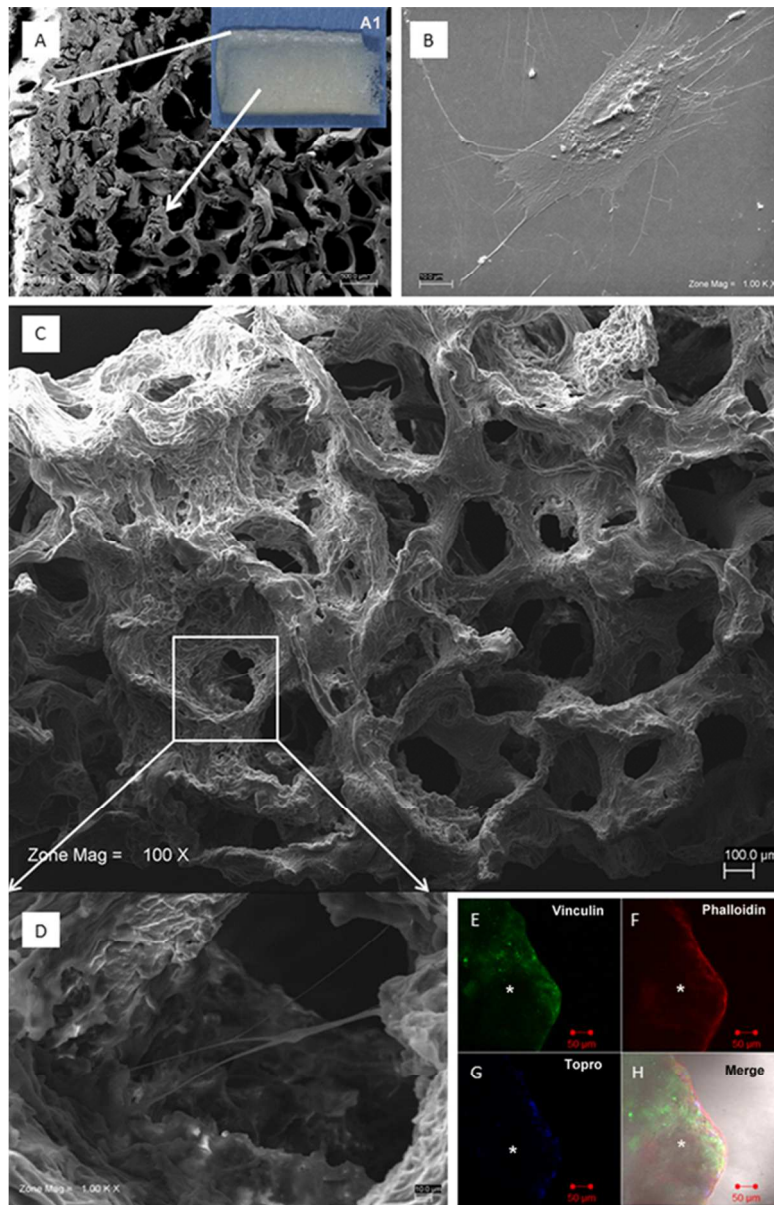


Cytofluorimetric analysis of hPDLSCs culture. The values are expressed as mean fluorescence ratio (MFI) obtained dividing the MFI of positive events by the MFI of negative events. In section A the numeric values of MFI ratio are the mean  $\pm$  standard deviation (SD) of three separate experiments using cells at 2nd passage.

MTT assay in hPDLSCs grown in vitro under undifferentiating condition, with (DB-ctrl@group) or without biomaterial (ctrl@group), over 24h, 48h, 72h, 1 week time-points. The proliferation rate was measured as the absorbance detected at 490 nm.

Trypan blue exclusion test show the proliferation rate and viability of hPDLSCs. In both tests MTT (B) and Trypan Blue (C) the cells seeded on the dual-block showed a slightly lower growth in all examined time-points. The Y-axis shows cell number, and X-axis shows culture time. Results are expressed as mean  $\pm$ SEM of three independent experiments for each patient.

88x69mm (300 x 300 DPI)

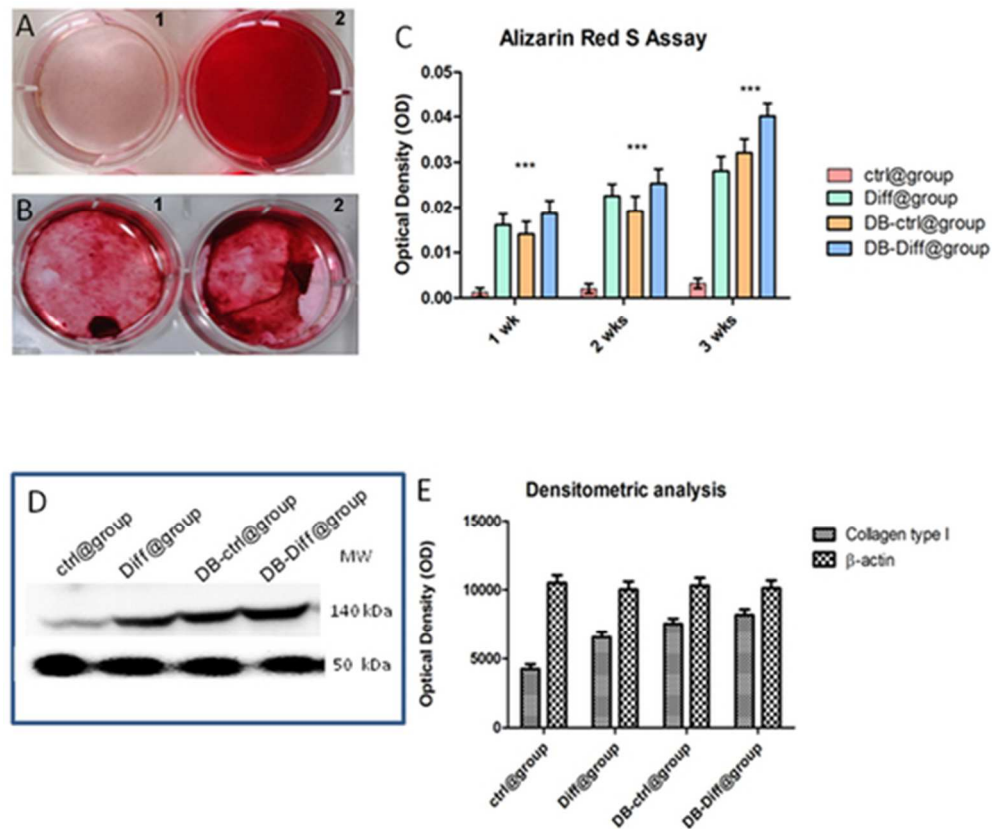


Scanning electron microscopy of Dual Block before grafting. (A) The cortical bone is anchored to cancellous bone; the biomaterial block, as commercially provided, is showed in the inset (A1). (B) Photomicrograph of a primary culture of human Periodontal Ligament Stem Cell (hPDLSC) line expanded ex vivo; it shows a morphological homogeneous fibroblast-like appearance with a stellate shape and elongated cytoplasmic processes. (C) Living un-induced hPDLSCs (DB-ctrl@group), after 24h of culture, grown on tridimensional scaffold. High magnification revealed hPDLSCs adhesion to substrate: in fact, confluent cells were observed on the biomaterial surface. (D) Cellular margin were indiscernible for the intimate contact between neighboring cells; cellular bridge was evident in the cancellous space. (E-H) Representative image of hPDLSCs seeded on 3D-biomaterial expressing vinculin and actin. Section E (green fluorescence) showed a punctate vinculin labelling in cells adhering to substrate. Rhoadamine -Phalloidin staining showed the spatial cytoskeleton of human periodontal ligament stem cells (red fluorescence, F). In section G it was possible to observe the nuclei stained with Topro (blue fluorescence). Section H indicated merged image with the triple staining of cells seeded on biomaterial. Asterisk: 3D-Dual Block.

1  
2  
3  
4  
5  
6  
7  
8  
9  
10  
11  
12  
13  
14  
15  
16  
17  
18  
19  
20  
21  
22  
23  
24  
25  
26  
27  
28  
29  
30  
31  
32  
33  
34  
35  
36  
37  
38  
39  
40  
41  
42  
43  
44  
45  
46  
47  
48  
49  
50  
51  
52  
53  
54  
55  
56  
57  
58  
59  
60

54x83mm (300 x 300 DPI)

Manuscript proof



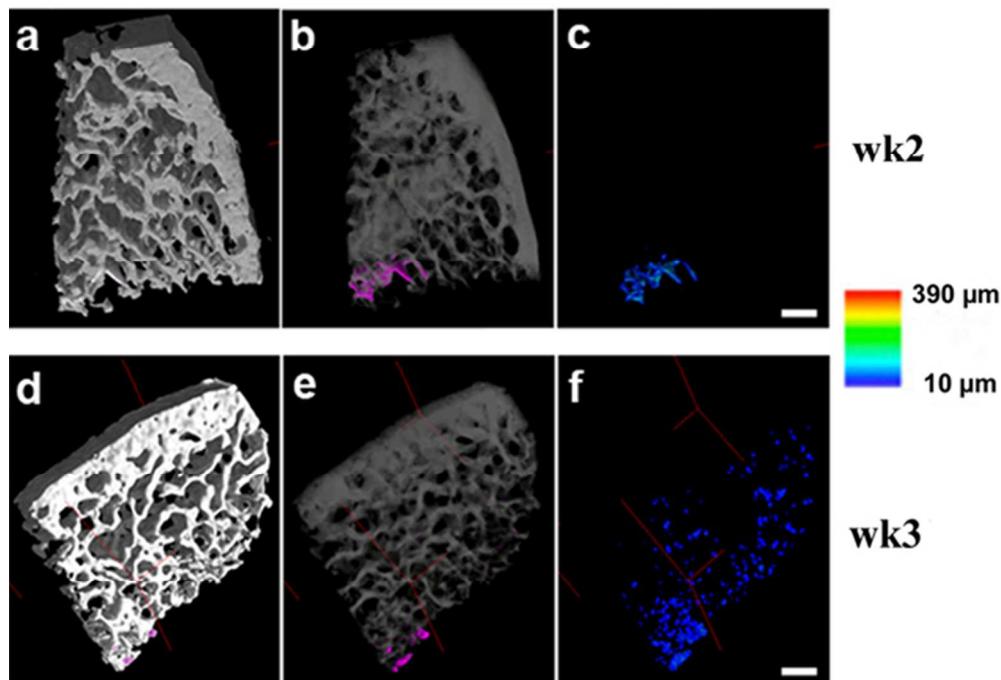
The osteogenic differentiation of hPDLS cells was evaluated as extracellular matrix mineralization for 21 days, in basal (A1 and B1) and osteogenic medium (A2 and B2), in absence (A) or presence (B) of the collagenated biomaterial. If a mineralized matrix is present in osteogenic induced cells (A2) also in absence of the scaffold, an evident mineralization was detected both in basal conditions (B1) and in osteogenic induction (B2) when the scaffold is present.

Mineralization of hPDLS cells, grown for 1, 2 and 3 weeks under osteogenic and basal conditions, with or without biomaterial, was evaluated by cell staining with Alizarin red S (ARS) and quantification of staining (C) via extraction with ammonium hydroxide at different commitment times. The amount of released dye is measured by a microplate reader at 405 nm. The values, expressed as units of optical density (O.D.), are the mean  $\pm$  SEM of three independent experiments, in which different cell samples were used.

Immunoblotting experiments and densitometric analysis of collagen type 1 showed an upregulation of protein in osteogenic induced cells respect to control. In DB-ctrl@group a quantity of the collagen type 1 protein similar to DB-diff@group was present indicating the osteoinductive properties of the biomaterial.  $\beta$ -actin represents a housekeeping protein (D and E).

45x38mm (300 x 300 DPI)

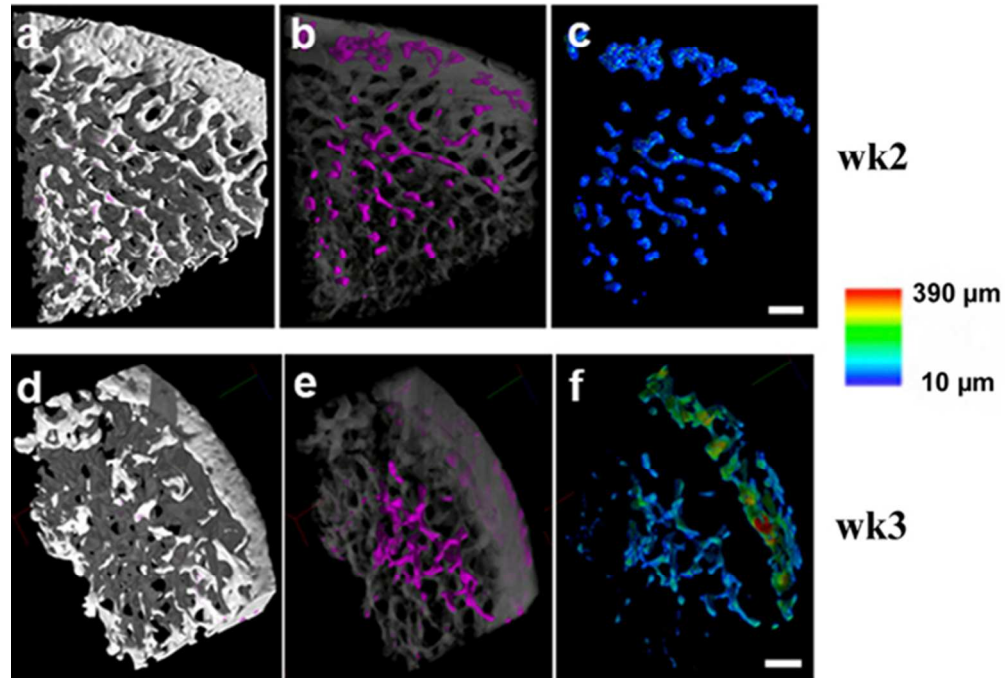
### Dual Block + PDLSCs in Basal Medium



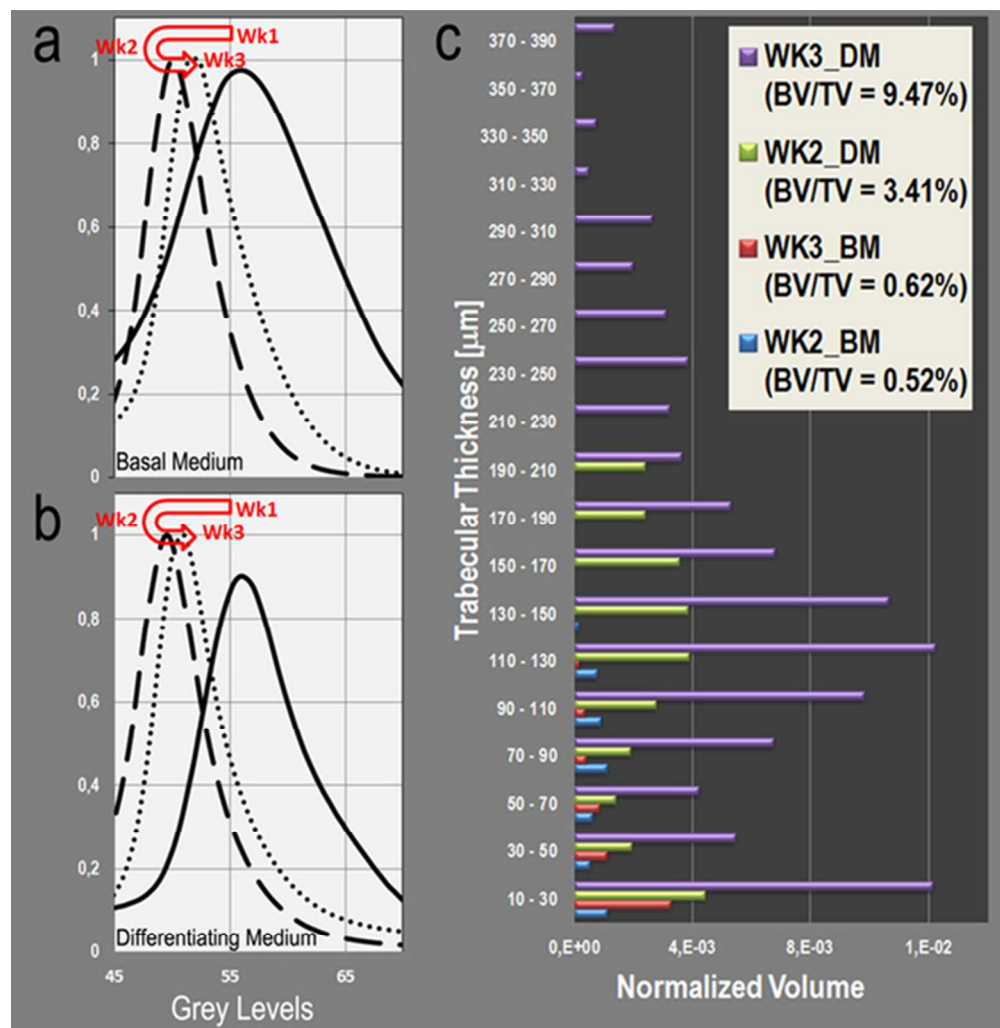
Dual block and hPDLSCs in basal medium. The interaction between cells and scaffold produces 3D Micro-CT images with two different phases, corresponding to different  $\delta$  (refractive index decrement) values. DB scaffolds are rendered in grey (panels a, b at wk2; panels d, e at wk3), whereas the contrast produced by cells - the newly-formed bone - is colored in magenta (panel b at wk2; panel e at wk3). Color map of bone thickness distribution at wk2 and wk3 are given in panel c and panel f, respectively. Thickness scale on the left. Bar: 500  $\mu\text{m}$ .

54x40mm (300 x 300 DPI)

### Dual Block + PDLSCs in Diff. Medium

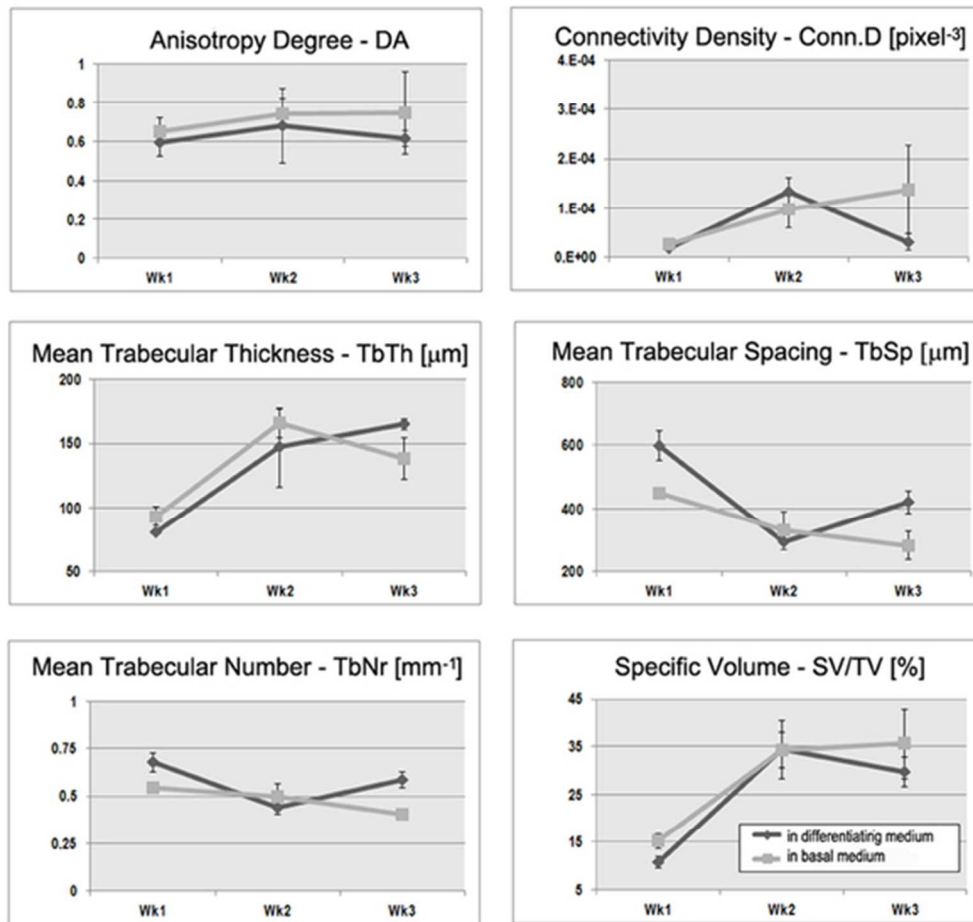


Dual block and hPDLSCs in osteogenic medium. The interaction between cells and scaffold produces 3D Micro-CT images with two different phases, corresponding to different  $\delta$  (refractive index decrement) values. DB scaffolds are rendered in grey (panels a, b at wk2; panels d, e at wk3), whereas the contrast produced by cells - the newly-formed bone - is colored in magenta (panel b at wk2; panel e at wk3). Color map of bone thickness distribution at wk2 and wk3 are given in panel c and panel f, respectively. Thickness scale on the left. Bar: 500  $\mu\text{m}$ .  
 54x39mm (300 x 300 DPI)



(a-b) Portion of the profile of the Intensity Counts vs. Grey Levels (proportional to the refractive index decrement  $\delta$ ). The integrated areas of the represented peaks correspond to the collagenated porcine Dual-block volume in scaffolds cultured in basal medium (panel a) and differentiating medium (panel b). In both media the contrast produced at wk2 of culture is lower than for wk1, but increases from wk2 to wk3. (c) Histograms of the distribution of the bone thickness in all the investigated samples at wk2 and wk3 of culture. The volume ratio ( $= BV/TV$ ) of the newly-formed bone structure (BV) to the total construct volume (TV) is reported in the top-right insert.

55x56mm (300 x 300 DPI)



Morphometric parameters investigated in scaffolds cultured with hPDLSCs, both in basal and differentiating media, after 1, 2 and 3 wks of culture: Anisotropy Degree (DA); Connectivity Density (Conn.D. – expressed in pixel<sup>-3</sup>); Mean Trabecular Thickness (TbTh - expressed in micrometers); Mean Trabecular Separation (TbSp - expressed in micrometers); Mean Trabecular Number (TbNr – per millimeter); Sample Volume (SV) to Total Volume (TV) ratio (SV/TV – expressed as a percentage).  
50x46mm (300 x 300 DPI)